Surfaces and Interfaces 49 (2024) 104445

Contents lists available at ScienceDirect

Surfaces and Interfaces

journal homepage: www.sciencedirect.com/journal/surfaces-and-interfaces

Dominant n-type conduction and fast photoresponse in BP/ MoS_2 heterostructures

Loredana Viscardi [a], Ofelia Durante [a], Sebastiano De Stefano [a], Kimberly Intonti [a], Arun Kumar [a], Aniello Pelella [b], Filippo Giubileo [c], Osamah Kharsah [d], Leon Daniel [d], Stephan Sleziona [d], Marika Schleberger [d,*], Antonio Di Bartolomeo [a,*]

[a] Department of Physics "E. R. Caianiello", University of Salerno, via Giovanni Paolo II, Fisciano, Salerno, 84084, Italy
[b] Department of Physics, University of Roma "Tor Vergata", Via Della Ricerca Scientifica, 1 - 00133, Rome, Italy
[c] CNR-SPIN, via Giovanni Paolo II, Fisciano, Salerno, 84084, Italy
[d] Fakultät für Physik and CENIDE, Universität Duisburg-Essen, Lotharstrasse 1, Duisburg D-47057, Germany

ARTICLE INFO

Keywords:
Van der Waals heterojunctions
Type II heterojunction
Heterojunction photoresponse
Band alignment
BP/MoS_2 Heterostructures

ABSTRACT

In recent years, van der Waals heterojunctions between two-dimensional (2D) materials have garnered significant attention for their unique electronic and optoelectronic properties and have opened avenues for innovative device architectures and applications. Among them, the heterojunction formed by black phosphorus (BP) and molybdenum disulfide (MoS_2) stands out as a promising candidate for advanced optoelectronic devices. This study unravels the interplay between BP, MoS_2, and Cr contacts to explain the electrical behavior of a BP/MoS_2 heterojunction showing rectifying behavior with dominant n-type conduction, and a high ON/OFF current ratio around 10^4 at ± 20 V. The higher unexpected current observed when applying a negative bias to either MoS_2 or BP side is elucidated by an energy band model incorporating a type II heterojunction at the BP/MoS_2 interface with Cr forming a Schottky contact with MoS_2 and an ohmic contact with BP. The BP/MoS_2 heterojunction shows pronounced photoresponse, linearly dependent on the incident laser power, with a responsivity of 100 μA/W under white light at 50 μW incident power. Time-resolved photocurrent measurements reveal a relatively fast response with characteristic rise times less than 200 ms. This work demonstrates that BP/MoS_2 van der Waals heterojunctions have unique electrical and photoresponse characteristics that are promising for advanced optoelectronic applications.

1. Introduction

Two-dimensional (2D) layered materials, including graphene, transition metal dichalcogenides (TMDCs), black phosphorus (BP), and hexagonal boron nitride (h-BN), have been widely exploited for the development of a new class of 2D heterojunction devices [1–7]. The absence of dangling bonds on the 2D material surface and the weak van der Waals (vdW) interactions between layers provide opportunities for constructing new functional devices, without the constraints of lattice matching [8]. Unlike conventional heterojunctions, 2D heterojunctions exploit only vdW interactions and can be realized without extra engineering to cope with lattice mismatches [9,10].

Researchers have explored various heterostructures, such as 2D p-n heterojunctions fabricated using vdW assembly of p-type WSe_2 and n-type MoS_2, demonstrating gate-tunable diode-like current rectification [11]. Heterostructures based on MoS_2 and other TMDCs, graphene or carbon nanotubes [12–23] have shown similar features. In the realm of these heterojunctions, rectification, and photovoltaic processes result from the establishment of either a Schottky or a p-n barrier that facilitates the efficient separation and collection of photocarriers. Binary and ternary inverters, leveraging p-n-p junctions comprising BP/ReS_2/BP and other structures, have showcased multifunctionality [24].

Moreover, 2D heterojunctions have been included in on-chip photonic integrated circuits for optical computing, communications, chemical/bio-sensing, and LiDARs [25]. For example, p-n heterojunctions of 2D materials on optical waveguides can be created by stacking few-layer BP and $MoTe_2$, where the ultrathin thickness and steep charge carrier gradient of these heterojunctions enable electrostatic doping to enhance rectification behavior and improve photodetection performance [26]. Similarly, BP/MoS_2 heterojunctions have

---

* Corresponding authors.
E-mail addresses: marika.schleberger@uni-due.de (M. Schleberger), adibartolomeo@unisa.it (A. Di Bartolomeo).

https://doi.org/10.1016/j.surfin.2024.104445
Received 19 April 2024; Received in revised form 2 May 2024; Accepted 5 May 2024

been proposed for high-performance sensing and energy harvesting applications in wireless power supply micro/nano-systems [27].

In the field of optoelectronics, photodetectors based on 2D materials offer advantages over traditional silicon-based ones, extending the detection range to the mid-IR spectral region [28]. Indeed, the band alignment of such layered structures can be controlled by strain, number of layers, chemical doping, and externally applied fields. The practical applications strongly depend on the type of band alignment. 2D material heterojunctions with large bandgap offsets and high built-in fields can achieve power conversion efficiencies exceeding 25 % and can be used for micro/nanoscale solar energy conversion. The formation of a type II heterojunction is desirable for photovoltaics and photodetectors because the conduction band minimum and the valence band maximum are in different materials [29].

In this context, MoS_2 as a large bandgap n-type and BP as a narrow bandgap p-type 2D semiconductor can be integrated to achieve large bandgap offsets, facilitating efficient rectifying behavior. Gate-tunable p-n diodes based on BP/MoS_2 vertical heterostructures have demonstrated significant rectification [9,10,19,27,30]. BP/MoS_2 heterojunctions have been exploited for the realization of tunnel field effect transistors (FETs) [31,32]. Furthermore, BP/MoS_2 heterojunctions have shown promising properties for photodetection. Photoresponsivities from few mA/W to A/W have been achieved with few-layer BP/MoS_2 heterojunctions [10,27,30].

In this work, we fabricate and investigate a BP/MoS_2 heterojunction to explore the electrical and optoelectronic features of the expected p-n junction. Indeed, the device displays rectifying behavior, with favorable ON/OFF current ratio representing the highest (lowest) current level achieved by the device. However, the heterostructure exhibits unexpected higher current when a negative bias is applied on either MoS_2 or BP side. This behavior is elucidated through a model that considers the band alignment of MoS_2, BP, and Cr, which is the metal used to contact the heterostructure. Indeed, it is shown that the formation of an electron Schottky barrier at the Cr/MoS_2 interface and the high hole barrier at the BP/MoS_2 interface play an important role in shaping the current-voltage characteristics of the device. Under illumination, the heterojunction exhibits a noteworthy increase in drain current, linearly depending on the incident laser power. Time-resolved photocurrent measurements reveal a relatively fast response with characteristic rise times less than 200 ms, and a responsivity of 100 μA/W at 50 μW incident laser power. The high responsivity and shorter relaxation time compared to similar MoS_2 devices imply an enhanced capability to generate and collect photo-charge, attributed to the presence of BP. Our findings valuably contribute to the understanding of van der Waals heterojunctions, necessary for future advances in 2D material-based electronic and optoelectronic devices.

2. Device fabrication

The MoS_2 flakes were grown on p-type doped silicon (p-Si) capped by 285 nm silicon dioxide (SiO_2) following an optimized variation of the procedure described by Pollman *et al.* [33,34]. For this work, the growth utilized atmospheric pressure chemical vapor deposition (APCVD) in a two-zone split tube furnace, employing argon (Ar) as a carrier gas. Ammonium heptamolybdate (AHM) solution served as the molybdenum precursor, while sulfur powder was placed in the upstream zone of the tube furnace. The temperature of the sulfur zone and AHM zone was set to 170 °C and 750 °C, respectively. After a growth time of 30 min, the process was halted, and the sample was allowed to cool down for 40–60 min. Few-layer BP flakes were obtained through mechanical exfoliation from bulk material onto a SiO_2/Si substrate. Then, selected BP flakes were transferred onto the SiO_2/Si substrate with the previously grown MoS_2 flakes using a dry stacking process that involved an aligned transfer platform (HQ graphene) and a polypropylene carbonate (PPC) film as the carrier. A micro-UV light maskless lithography (Smartprint UV) was employed to define the contact patterns. Cr (10 nm) and Au (110 nm) were deposited using thermal and electron evaporation to form the Cr/Au source and drain electrodes with low contact resistance [35]. Fig. 1a illustrates the schematic of the device and its electrical connections. The optical image in Fig. 1b provides a top view of the device, showing the overlap of the BP and MoS_2 flakes. In Fig. 1c, a false-color Atomic Force Microscope (AFM, NaioAFM by Nanosurf AG) image of the device is presented. From this image, multiple profiles were extracted to estimate the thicknesses of both BP and MoS_2. Representative height profiles are shown in Fig. 1d, indicating a BP thickness of ∼150 nm and a MoS_2 thickness of ∼1.9 nm. Considering the monolayer thicknesses of 0.7 nm for BP [36], it can be deduced that BP exists in the form of multilayer film. In the case of MoS_2, the measured thickness is typical for a monolayer despite the apparent difference to the nominal thickness of 0.67 nm [37], which can be attributed to process residues and ubiquitous water layers [38,39]. To avoid any unambiguity, the monolayer nature of MoS_2 was confirmed by PL measurements (see Fig. 1e).

Fig. 1e illustrates the photoluminescence (PL) from MoS_2 and from the BP/MoS_2 heterojunction. A noticeable PL quenching from the region of the BP/MoS_2 heterojunction is evident. The reduction of the peak intensity compared to the pristine MoS_2 material is attributed to exciton dissociation and charge transfer at the BP/MoS_2 interface [30]. The Raman spectra of MoS_2, BP, and the BP/MoS_2 heterojunction are presented in different colors in Fig. 1f.

Peaks observed at approximately 383 cm^{-1} and 408 cm^{-1} correspond to the E^1_{2g} and A_{1g} phonon modes of MoS_2, respectively. Peaks observed at around 361 cm^{-1}, 439 cm^{-1}, and 466 cm^{-1} correspond to the A^1_g, B_{2g}, and A^2_g phonon modes of BP [9,10]. Both MoS_2 and BP peaks are evident in the Raman spectrum from the overlapping region (black curve in Fig. 1f) with a minimal shift in the Raman modes of MoS_2 compared to the reference ones.

Indeed, the difference of modes in both the MoS_2 spectrum and the BP/MoS_2 heterojunction spectrum is 21 cm^{-1}, as indicated in Fig. 1f. This difference is consistent with values reported in the literature for monolayer flakes of MoS_2 [40–42]. It is worth noting that this consistency is within the expected experimental error of 0.5 cm^{-1}. Additionally, the use of low laser power during the measurement may have influenced the observed modes, potentially affecting the accuracy of the measurement. Furthermore, from the full width at half maximum (FWHM) of the two main Raman modes of the MoS_2 flake, it can be inferred that it exhibits a polycrystalline structure (see Supplementary Information, Figure S1). The Raman spectra confirm the high quality of the flakes and the formation of a BP/MoS_2 heterojunction.

3. Results and discussion

We performed the electrical characterization of the BP/MoS_2 heterostructure in vacuum, at a pressure of 0.7 mbar, to prevent the degradation of BP by oxidation [43]. The electrical measurements were performed in two-probe configuration (Fig. 1a). The Cr/Au source and drain were grounded and biased at a voltage (V_{ds}) ranging from −20 to 20 V, respectively. Figs. 2a and 2b illustrate the drain current (I_d) as a function of V_{ds} when the drain, i.e. the forcing electrode, is connected to the MoS_2 or the BP flake, respectively. The black curves, which in both plots represent the device characteristic in dark, exhibit good rectifying behavior with the higher current occurring at negative voltages and the ON/OFF current ratio, evalued at ± 20 V, of the order of 10^4 when the drain is connected either to MoS_2 or BP.

Figs. 2a and 2b also include the current-voltage (I-V) characteristics of the BP/MoS_2 heterostructure measured under illumination by a white laser (450–2400 nm wavelength range) at different incident laser powers, ranging from 10 to 50 μW. At both positive and negative biases, an increase in photocurrent with increasing incident laser power occurs, emphasizing a strong photoresponse.

Similarly, Figs. 2c and 2d display the output characteristics, which show I_d as a function of V_{ds} at different gate voltage (V_{gs}). With the drain

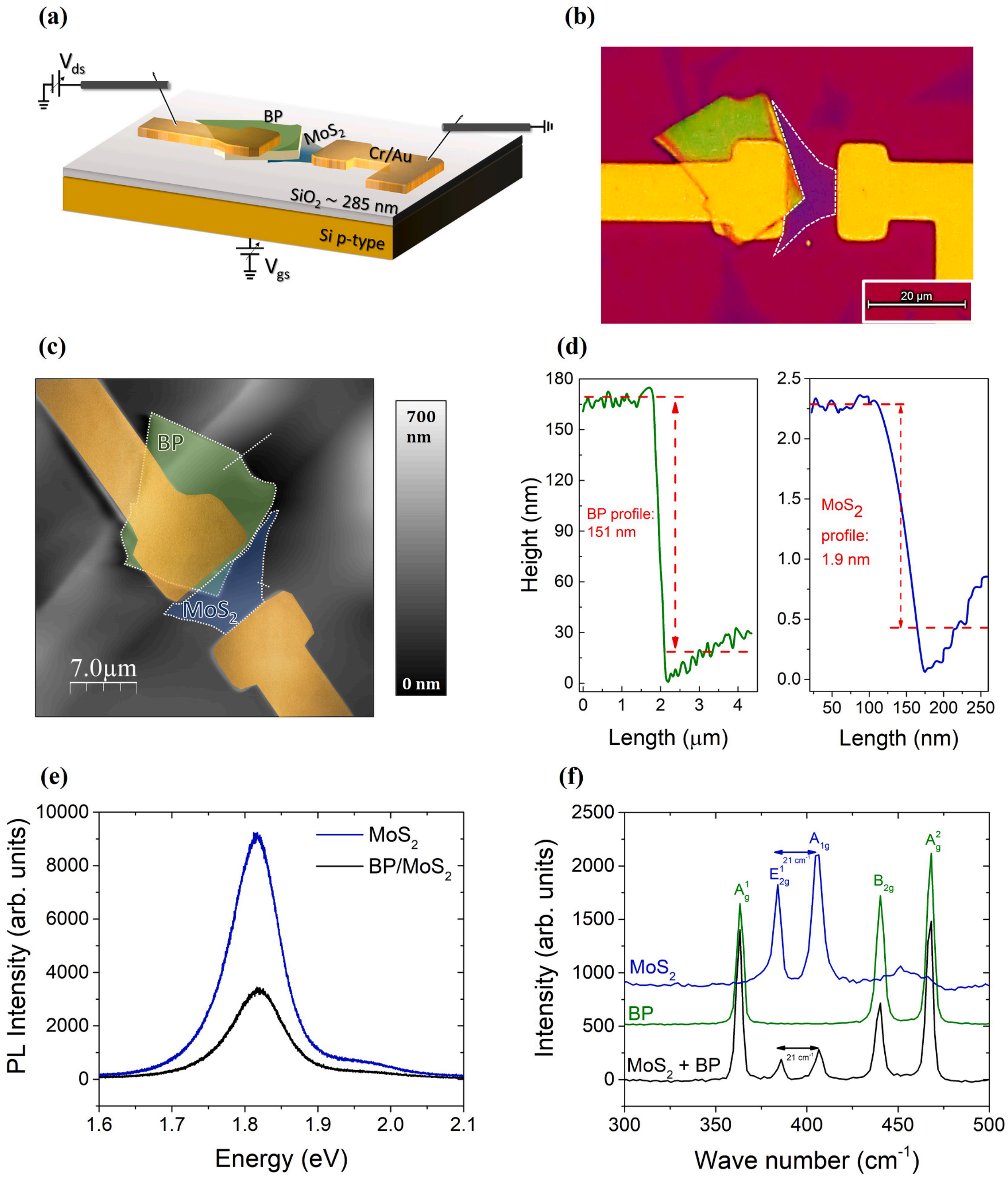

Fig. 1. (a) Schematic of the device with the electrical measurement setup. (b) Processed optical image and (c) AFM image (false-color) of the BP/MoS_2 heterojunction contacted with Cr/Au leads. (d) AFM profiles of BP (green, left panel) and MoS_2 (blue, right panel). (e) PL spectra of MoS_2 (blue) and BP/MoS_2 heterojunction (black). (f) Raman spectrum of the MoS_2 (blue), BP (green), and BP/MoS_2 heterojunction (black).

on either MoS_2 or BP, I_d rises when V_{gs} increases from 0 to 30 V, indicating the dominant n-type behavior of the BP/MoS_2 device. Moreover, a loss of rectification is observed, particularly when the drain is connected to BP (see Fig. 2d). The ability of the gate to modulate the current and the rectifying behavior of the device is noteworthy; it shows that the gate voltage can affect the Schottky barriers at the interface Cr/MoS_2 in the BP/MoS_2 device and lead to a more balanced bidirectional charge transport [44].

The presented electrical behavior of the BP/MoS_2 heterostructure differs from the usual behavior reported in the literature [9,10,19,26,27,30]. Surprisingly, the current reaches the highest values at negative V_{ds}, regardless of the drain being on MoS_2 or BP. We notice that a similar behavior has been reported for MoS_2 transistors with asymmetric contacts [45,46]. These results can be explained by considering the band alignment of the two involved semiconductors and Cr that is the metal used for the source and drain electrodes. Fig. 3a depicts the band diagrams of MoS_2 and BP, referred to the vacuum level at thermal equilibrium. Considering the thickness of the two flakes extracted previously, the work function (Φ), electron affinity (χ), and energy bandgap (E_{gap}) for MoS_2 are 4.5, 4.2, and 1.8 eV [10,47–49], while for BP, they are 4.2, 4, and 0.3 eV [10,43,50], respectively. According to Anderson's rule, the combination of MoS_2 and BP results in the formation of a staggered gap heterojunction (type II heterojunction) [10,51], as depicted in Fig. 3b. It can be noted that at the BP/MoS_2 interface there is a barrier for electrons around 0.15 eV that cannot significantly hamper the electron flow. The band bending favors the accumulation of electrons from MoS_2 and holes from BP at the BP/MoS_2 interface; thus, electrons that enter the BP region surmounting the small barrier can

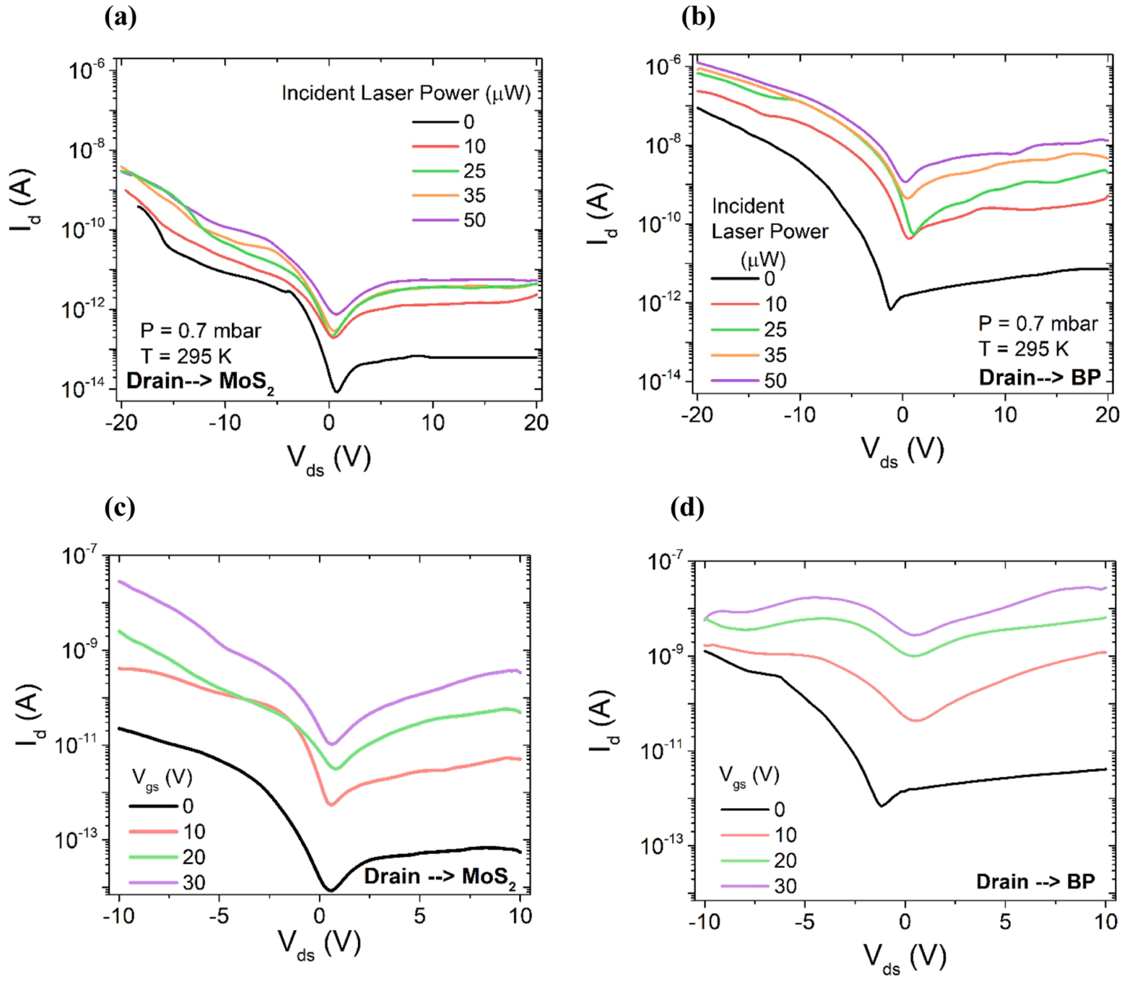

Fig. 2. I-V in dark (black curve) and at different incident laser powers (colored curves) at $T = 295$ K and $P = 0.7$ mbar of the BP/MoS_2 heterostructure with the drain connected to (a) MoS_2 and (b) BP. Output characteristics at $T = 295$ K and $P = 0.7$ mbar of the BP/MoS_2 heterostructure at fixed V_{gs} between 0 and 30 V with the forcing electrode connected to (c) MoS_2 and (d) BP.

recombine with holes. The recombination rate increases when BP is positively biased (see Fig. 3c) with respect to MoS_2 as BP bands move down, and more electrons and holes are injected in the interface region. Vice versa, when BP is negatively biased (see Fig. 3d) with respect to MoS_2, the current from the BP/MoS_2 heterojunction is mainly due to electron-hole generation and electron injected from the Cr contact that reach the BP/MoS_2 overlap region. Since the lowest energy state for holes is on the BP side and the lowest energy state for electrons is on the MoS_2 side of the heterojunction, charge separation can readily occur, causing also a significative photoresponse, as observed in Fig. 2, when the device is illuminated with white light (see Fig. 3e) [52].

The Fermi level of Cr is also indicated in the schematic in Figure 3b; its work function is 4.5 eV [53]. As indicated in the Supplementary Information (see Figures S2a,b) and as reported in many other works, Cr forms an ohmic contact with BP [54,55]. The ohmic contact is due to the favorable alignment of the Cr Fermi level with the top of the valence band of BP which enables hole injection. Moreover, it has been reported that, due to possible pinning effect, the electron barrier formed by Cr with multilayer BP can decrease below 0.1 eV with the increasing number of layers [56]. Conversely, the combination of MoS_2 and Cr results in the formation of a Schottky contact for electrons, which is characterized by a barrier that is 0.4–0.5 eV [57,58]. The presence of a Schottky barrier at the Cr/MoS_2 interface is discussed in the Supplementary Information, along with the electrical characterization of a MoS_2 FET with Cr/Au electrodes (see Figures S2c-f). The Schottky barrier at the Cr/MoS_2 interface limits the electron flow when the drain on BP is positively biased. In this case, the current in the device is limited by electron injection over the Cr/MoS_2 Schottky barrier and electron/hole recombination at the BP/MoS_2 interface.

Vice versa, when the drain on BP is negatively biased, the current flow is due to electron injection over the low Cr/BP barrier and electron-hole generation in the MoS_2/BP depletion region, resulting in a total current higher than in the previous case as the electron barrier at the Cr/BP is lower than at Cr/MoS_2 interface. Similarly, electrons are easily injected into the MoS_2 conduction band and recombine with holes in BP at the BP/MoS_2 interface when the drain on MoS_2 is negatively biased, thus yielding a pronounced current. Instead, with a positive bias on MoS_2, the electron-hole generation current at BP/MoS_2 interface limits the current flow; in this case, there is no hole current because of the high barrier for holes at the Cr/MoS_2 interface.

According to the just described model, the charge flow in the device is dominated by the electron flow in MoS_2, which is also the most resistive component of the heterojunction. The contact resistance was estimated to be 8.9×10^{-3} Ωm for Cr/BP and 2 Ωm for Cr/MoS_2, as described in the Supplementary Information. This is the main reason for the overall n-type conducting behavior evidenced by the effect of the gate voltage in Figs. 2c and 2d. However, we highlight that, related to the narrower bandgap, most of the electron-hole (photo)generation and recombination processes occur in BP, which plays a significant role also in enhancing the photoresponse and the speed of the BP/MoS_2 device.

To investigate the BP/MoS_2 heterojunction as a photodetector, we performed time-resolved measurements to study the photocarrier

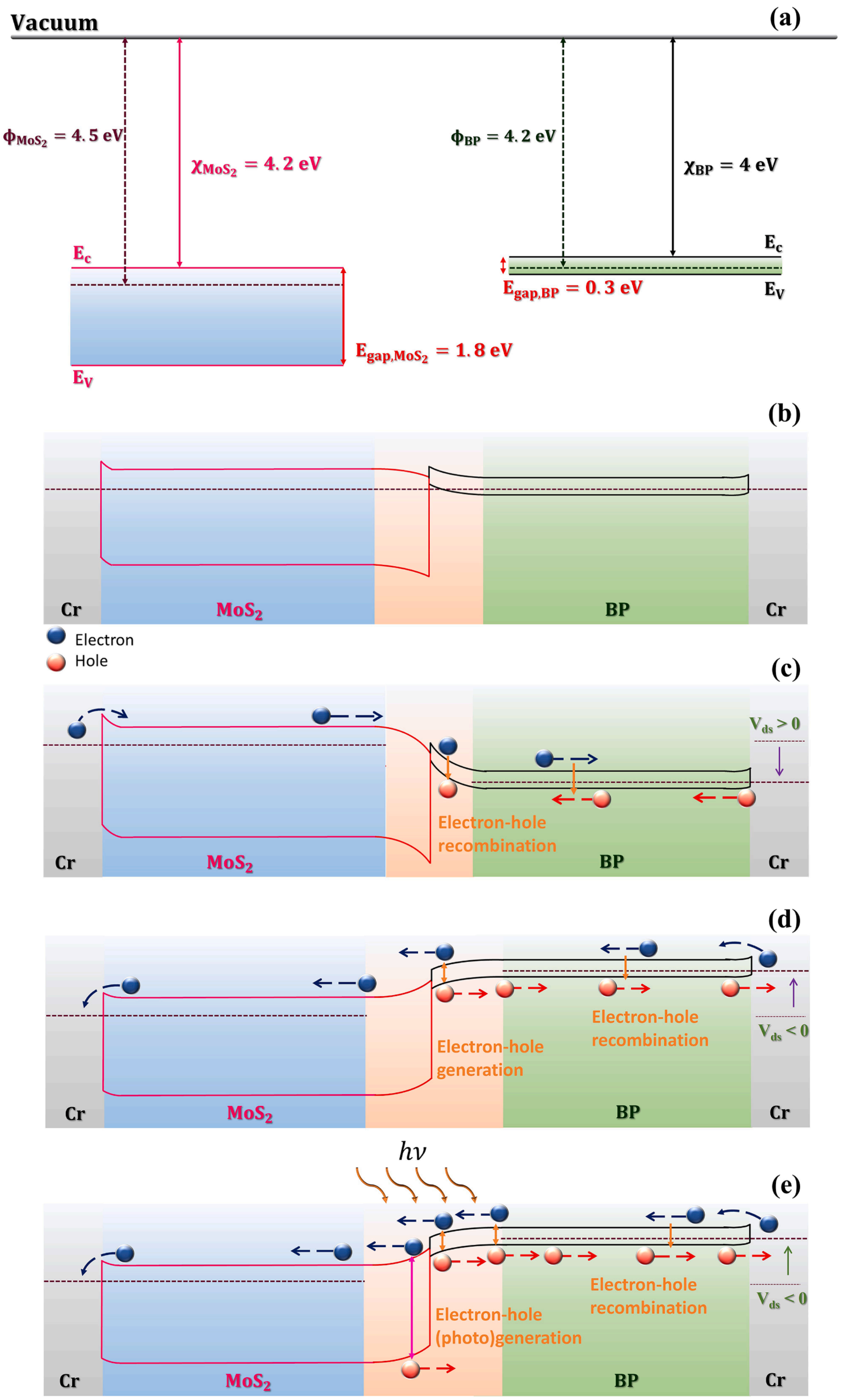

Fig. 3. (a) Band profiles of MoS_2 (light blue) and BP (green) when the two flakes are separated. The work function and the electron affinity of MoS_2 and BP are referred to the vacuum level. Band alignment of BP/MoS_2 heterojunction and Cr (b) in thermal equilibrium state, (c) with a positive bias on BP, (d) with a negative bias on BP, and (e) with a negative bias on BP under illumination (the Cr contact on MoS_2 is assumed to be grounded).

dynamics under illumination by a supercontinuum white laser (450–2400 nm wavelength range, Superk Compact, NKT Photonics). Heterojunction-based photodetectors are renowned for their high photoresponse compared to phototransistors, primarily because photoexcited carriers are easily separated and transported in the depletion layer of the junction [9]. Therefore, we illustrate the time-dependent nature of the photocurrent, I_{ph}, as a function of time with the drain on the BP side at two distinct voltage biases, i.e. $V_{ds} = 5$ V (Fig. 4a) and $V_{ds} = -5$ V (Fig. 4b), under exposure to 30 s laser pulses of increasing power. As expected from the already discussed band model, due to the favorable separation and collection of photogenerated electron-hole pairs, the device showcases greater photocurrent at negative V_{ds}. Moreover, these pulses can be fitted by a double exponential growth/decay in the rising and falling part, $I_{ph} = I_0 + a_1 \exp\left(-\frac{t-t_0}{\tau_1}\right) + a_2 \exp\left(-\frac{t-t_0}{\tau_2}\right)$, as shown both in Ref. [37] and by the red dashed curve in Figure S4a-b in the Supplementary Information.

The photocurrent exhibits an average characteristic rise time (τ_1) of ~300 ms and a decay time (τ_2) of ~1400 ms at $V_{ds} = 5$ V (Fig. 4c), and a rise time (τ_1) of ~200 ms and a decay time (τ_2) of ~1000 ms at $V_{ds} = -5$ V (Fig. 4d). Notably, both photocurrent rise (τ_1) and decay (τ_2) times are smaller than those observed in recently reported phototransistors with

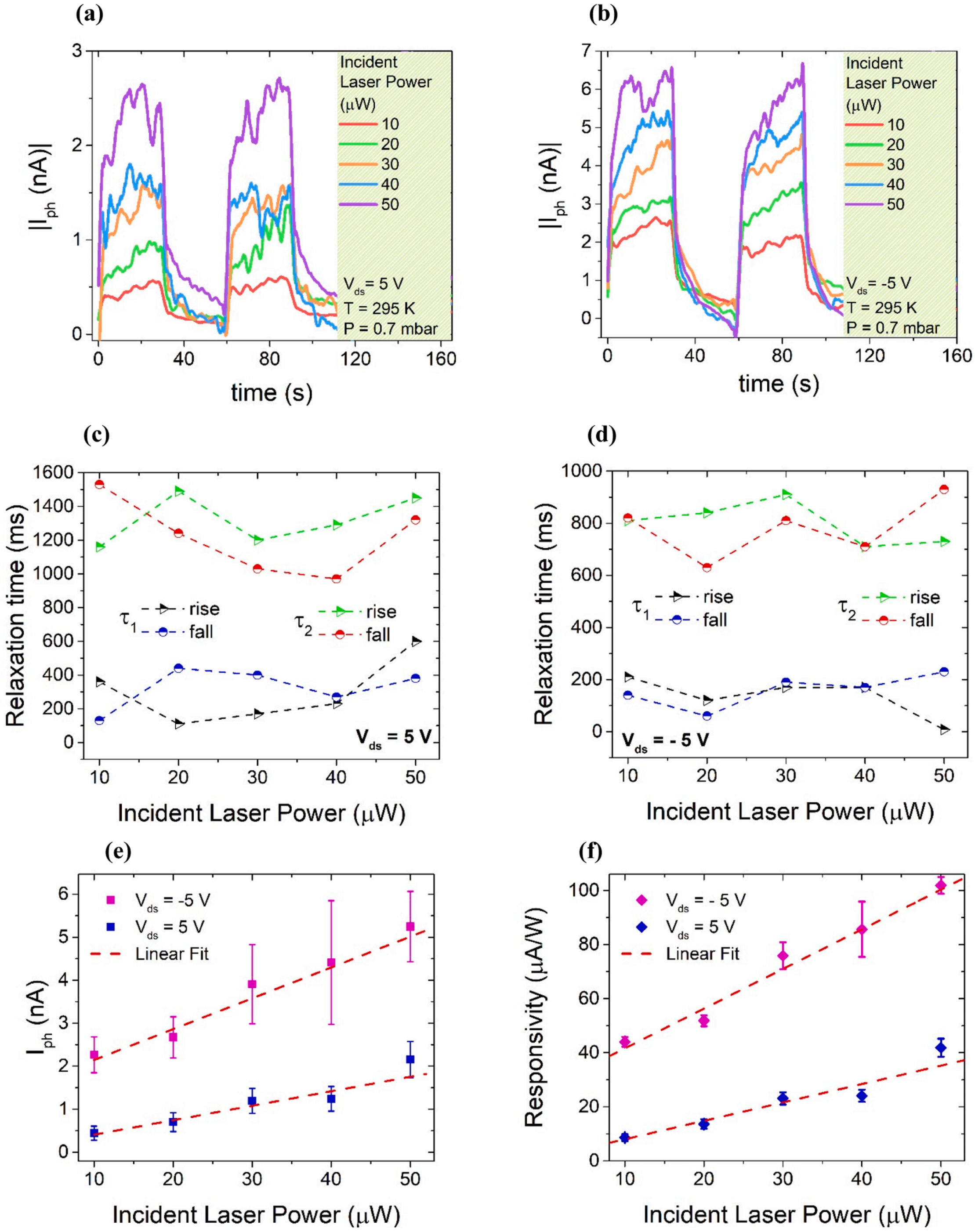

Fig. 4. Photocurrent vs time at $T = 295$ K and $P = 0.7$ mbar with the drain electrode on BP and at fixed voltage (a) $V_{ds} = 5$ V and (b) $V_{ds} = -5$ V. Relaxation time as a function of the incident laser power for the rising and falling part of the pulses at (c) $V_{ds} = 5$ V and (d) $V_{ds} = -5$ V. (e) Photocurrent and (f) Responsivity vs incident laser power at $V_{ds} = 5$ V (blue) and $V_{ds} = -5$ V (magenta). In (e) and (f), the red dashed curves represent a linear fit.

MoS_2 channel [37]. These shorter relaxation times suggest that the faster photoresponse of the BP/MoS_2 device is due to the presence of BP which has a mobility more than an order of magnitude higher than MoS_2 [37, 43,59]. We point out that the response time can be further lowered by reducing the carrier path to the electrodes for instance by reducing the BP or MoS_2 extensions out of the junction region or by changing the device layout to obtain a truly vertical device.

Fig. 4e shows that the photocurrent, which results to be higher at negative V_{ds}, depends linearly on the incident laser power (from 10 to 50 μW). This is a desirable feature in a photodetector, related to its ability to distinguish varying light intensities. The linear dependence of photocurrent on the incident laser power aligns with results reported for both phototransistors with 2D single [37,60] or heterojunction channel [26, 30].

Finally, we determined the device responsivity as a function of the incident laser power as shown in Fig. 4f. The responsivity is calculated as $R= (I_{light}\text{- } I_{dark})/(P_{incident})$, where $P_{incident} = (P_{laser}/S_{spot}) * S_{active}$, P_{laser} is the maximum laser power, $S_{spot} = 1\ mm^2$, and $S_{active} = 490\ \mu m^2$ is the active area, i.e., the area covered by semiconducting material between the two electrodes, extracted from the optical image in Figure 1(b). At both positive and negative V_{ds}, the responsivity increases linearly with the incident laser power up to 100 μA/W at $V_{ds} = -5$ V and $P_{incident} = 50$ μW, as depicted by the linear fit in Fig. 4f. The lower responsivity compared to results in the literature [10,27,30] (see Table 1) can be attributed to monolayer MoS_2. The responsivity can be increased by enhancing light absorption using multilayer MoS_2.

4. Conclusions

In this study, the electrical transport and photo response properties of a BP/MoS_2 heterojunction were studied. The heterostructure exhibited good rectifying behavior. Differently from a conventional p-n junction, the BP/MoS_2 heterostructure showed an unexpected higher current when a negative voltage bias was applied on either BP or MoS_2 side. The observed behavior was explained through an energy band model including a type II BP/MoS_2 heterojunction with Schottky and ohmic Cr contacts on MoS_2 and BP, respectively.

The photoresponse of the heterojunction, investigated by time-resolved measurements, revealed a linear increase in drain current with the incident laser power and relatively faster photoresponse times compared to MoS_2-based phototransistors, attributed to the high mobility that characterizes BP. Moreover, a responsivity of 100 μA/W at 50 μW incident power confirmed efficient carrier separation and transport. Overall, the results on the BP/MoS_2 heterostructure demonstrated promising electrical and optoelectronic characteristics that can contribute to the understanding of van der Waals heterojunctions for future advances in optoelectronic devices based on 2D materials.

CRediT authorship contribution statement

Loredana Viscardi: Writing – original draft, Visualization, Methodology, Investigation, Formal analysis, Conceptualization. **Ofelia Durante:** Writing – original draft, Visualization, Methodology, Investigation, Formal analysis, Conceptualization. **Sebastiano De Stefano:** Visualization, Software, Data curation. **Kimberly Intonti:** Visualization, Software, Data curation. **Arun Kumar:** Software, Data curation. **Aniello Pelella:** Visualization, Software, Data curation. **Filippo Giubileo:** Visualization, Validation, Software, Funding acquisition, Data curation. **Osamah Kharsah:** Methodology, Investigation. **Leon Daniel:** Methodology, Investigation. **Stephan Sleziona:** Methodology, Investigation. **Marika Schleberger:** Writing – review & editing, Validation, Supervision, Resources, Project administration, Funding acquisition, Conceptualization. **Antonio Di Bartolomeo:** Writing – review & editing, Validation, Supervision, Resources, Project administration, Funding acquisition, Conceptualization.

Table 1
BP/MoS_2 responsivities from literature and this work.

Reference	BP/MoS_2 Thickness	Power/Power density	Wavelength	Responsivity
Ref. [10]	5.9 nm/4.6 nm	0.75 nW	500 nm	8500 mA/W
Ref. [27]	20.71 nm/7.05 nm	7.2 mW	830 nm	27.43 mA/W
Ref. [30]	8 nm/3 nm	3.6 W cm^{-2}	375–1550 nm	3.0 × 10^5 A/W
This work	150 nm/0.67 nm	50 μW	450–2400 nm	0.1 mA/W

Declaration of competing interest

The authors declare that they have no known competing financial interests or personal relationships that could have appeared to influence the work reported in this paper.

Data availability

The raw/processed data required to reproduce these findings cannot be shared at this time due to technical or time limitations. However, the raw/processed data can be requested to the corresponding author at any time.

Funding Sources

A.D.B. and A.K. acknowledge the financial support from the European Union's REACT-EU PON Research and Innovation 2014–2020, Ministerial Decree 1062/2021, and from the University of Salerno, with grant ORSA223384 and ORSA235199. M.S., S.S., L.V., O.D. acknowledge support from the Deutsche Forschungsgemeinschaft (DFG, German Research Foundation - project No. 278162697-SFB 1242) in the frame of the project "Particle-Induced Excitations" (C05) CRC 1242 and by project No. 29784087. M.S. O.K., L.D. acknowledge financial support from the DFG within the IRTG 2803: 2D Mature, project No. 461605777. M.S. O.K., L.D., S.S., L.V., O.D., acknowledge support by the clean room staff of A. Lorke, especially G. Prinz.

Supplementary materials

Supplementary material associated with this article can be found, in the online version, at doi:10.1016/j.surfin.2024.104445.

References

[1] M. Huang, S. Li, Z. Zhang, X. Xiong, X. Li, Y. Wu, Multifunctional high-performance van der waals heterostructures, Nature Nanotech 12 (12) (2017) 1148–1154, https://doi.org/10.1038/nnano.2017.208.

[2] S.K. Behura, C. Wang, Y. Wen, V. Berry, Graphene–semiconductor heterojunction sheds light on emerging photovoltaics, Nat. Photonics 13 (5) (2019) 312–318, https://doi.org/10.1038/s41566-019-0391-9.

[3] K.S. Novoselov, A. Mishchenko, A. Carvalho, A.H. Castro Neto, 2D materials and van der waals heterostructures, Science 353 (6298) (2016) aac9439, https://doi.org/10.1126/science.aac9439.

[4] J. Ren, P. Innocenzi, 2D boron nitride heterostructures: recent advances and future challenges, Small Struct. 2 (11) (2021) 2100068, https://doi.org/10.1002/sstr.202100068.

[5] Z. Yang, J. Hao, Recent progress in black-phosphorus-based heterostructures for device applications, Small Methods 2 (2) (2018) 1700296, https://doi.org/10.1002/smtd.201700296.

[6] A. Di Bartolomeo, Emerging 2D materials and their van der waals heterostructures, Nanomaterials 10 (3) (2020) 579, https://doi.org/10.3390/nano10030579.

[7] C. Alvarado Chavarin, C. Strobel, J. Kitzmann, A. Di Bartolomeo, M. Lukosius, M. Albert, J. Bartha, C. Wenger, Current modulation of a heterojunction structure by an ultra-thin graphene base electrode, Materials (Basel) 11 (3) (2018) 345, https://doi.org/10.3390/ma11030345.

[8] A.K. Geim, I.V. Grigorieva, Van Der Waals Heterostructures, Nature 499 (7459) (2013) 419–425, https://doi.org/10.1038/nature12385.

[9] L. Ye, H. Li, Z. Chen, J. Xu, Near-infrared photodetector based on MoS_2 /black phosphorus heterojunction, ACS Photonics 3 (4) (2016) 692–699, https://doi.org/10.1021/acsphotonics.6b00079.

[10] X. Jiang, M. Zhang, L. Liu, X. Shi, Y. Yang, K. Zhang, H. Zhu, L. Chen, X. Liu, Q. Sun, D.W. Zhang, Multifunctional black phosphorus/MoS_2 van Der waals heterojunction, Nanophotonics 9 (8) (2020) 2487–2493, https://doi.org/10.1515/nanoph-2019-0549.

[11] M.-Y. Li, Y. Shi, C.-C. Cheng, L.-S. Lu, Y.-C. Lin, H.-L. Tang, M.-L. Tsai, C.-W. Chu, K.-H. Wei, J.-H. He, W.-H. Chang, K. Suenaga, L.-J. Li, Epitaxial growth of a monolayer WSe_2 -MoS_2 lateral p-n junction with an atomically sharp interface, Science 349 (6247) (2015) 524–528, https://doi.org/10.1126/science.aab4097.

[12] S. Hu, S. Ju, C. Shao, J. Guo, B. Xu, M. Ohnishi, J. Shiomi, Ultimate impedance of coherent heat conduction in van der waals graphene-MoS2 heterostructures, Mater. Today Phys. 16 (2021) 100324, https://doi.org/10.1016/j.mtphys.2020.100324.

[13] Y. Gong, J. Lin, X. Wang, G. Shi, S. Lei, Z. Lin, X. Zou, G. Ye, R. Vajtai, B. I. Yakobson, H. Terrones, M. Terrones, B.K. Tay, J. Lou, S.T. Pantelides, Z. Liu, W. Zhou, P.M Ajayan, Vertical and In-Plane heterostructures from WS2/MoS2 monolayers, Nature Mater 13 (12) (2014) 1135–1142, https://doi.org/10.1038/nmat4091.

[14] G. Xiong, J. Lu, R. Wang, Z. Lin, S. Lu, J. Li, Z. Tong, Z. Qiu, K. Chen, Y. Sun, F. Tian, C. Wang, A MoS2/BAs Heterojunction as photodetector, Mater. Today Phys. 42 (2024) 101360, https://doi.org/10.1016/j.mtphys.2024.101360.

[15] Y. Chen, X. Wang, G. Wu, Z. Wang, H. Fang, T. Lin, S. Sun, H. Shen, W. Hu, J. Wang, J. Sun, X. Meng, J. Chu, High-performance photovoltaic detector based on $MoTe_2$ /MoS_2 van der waals heterostructure, Small 14 (9) (2018) 1703293, https://doi.org/10.1002/smll.201703293.

[16] Y. Gong, S. Lei, G. Ye, B. Li, Y. He, K. Keyshar, X. Zhang, Q. Wang, J. Lou, Z. Liu, R. Vajtai, W. Zhou, P.M. Ajayan, Two-step growth of two-dimensional WSe_2 /$MoSe_2$ heterostructures, Nano Lett. 15 (9) (2015) 6135–6141, https://doi.org/10.1021/acs.nanolett.5b02423.

[17] F. Wang, Z. Wang, K. Xu, F. Wang, Q. Wang, Y. Huang, L. Yin, J. He, Tunable GaTe-MoS_2 van Der Waals p–n junctions with novel optoelectronic performance, Nano Lett. 15 (11) (2015) 7558–7566, https://doi.org/10.1021/acs.nanolett.5b03291.

[18] N. Zhang, F. Tan, L. Qi, J. An, M. Che, Y. Shi, Y. Li, Z. Shi, X. Sun, S. Li, D. Li, Switchable operating modes enable low power consumption and improved gas sensing efficiency in MoS2/BP heterojunction, Sens. Actuators B 396 (2023) 134620, https://doi.org/10.1016/j.snb.2023.134620.

[19] Y. Deng, Z. Luo, N.J. Conrad, H. Liu, Y. Gong, S. Najmaei, P.M. Ajayan, J. Lou, X. Xu, P.D. Ye, Black phosphorus–monolayer MoS_2 van der waals heterojunction p–n diode, ACS Nano 8 (8) (2014) 8292–8299, https://doi.org/10.1021/nn5027388.

[20] Z.H. Xu, L. Tang, S.W. Zhang, J.Z. Li, B.L. Liu, S.C. Zhao, C.J. Yu, G.D. Wei, 2D MoS2/CuPc heterojunction based highly sensitive photodetectors through ultrafast charge transfer, Mater. Today Phys. 15 (2020) 100273, https://doi.org/10.1016/j.mtphys.2020.100273.

[21] Y. Zhang, C. Wu, X. Zhou, J. Li, X. Tao, B. Liu, J. Chen, Y. Chang, G. Tong, Y. Jiang, Hetero-integrated MoS2/CsPbBr3 photodetector with enhanced performance via combinational modulation of grain boundary passivation and interfacial carrier separation, Mater. Today Phys. 36 (2023) 101179, https://doi.org/10.1016/j.mtphys.2023.101179.

[22] D. Jariwala, V.K. Sangwan, C.-C. Wu, P.L. Prabhumirashi, M.L. Geier, T.J. Marks, L. J. Lauhon, M.C. Hersam, Gate-tunable carbon nanotube–MoS_2 heterojunction p-n diode, Proc. Natl. Acad. Sci. U.S.A. 110 (45) (2013) 18076–18080, https://doi.org/10.1073/pnas.1317226110.

[23] M.-L. Tsai, S.-H. Su, J.-K. Chang, D.-S. Tsai, C.-H. Chen, C.-I. Wu, L.-J. Li, L.-J. Chen, J.-H. He, Monolayer MoS_2 heterojunction solar cells, ACS Nano 8 (8) (2014) 8317–8322, https://doi.org/10.1021/nn502776h.

[24] Y. Meng, W. Wang, W. Wang, B. Li, Y. Zhang, J. Ho, Anti-Ambipolar heterojunctions: materials, devices, and circuits, Adv. Mater. (2023) 2306290, https://doi.org/10.1002/adma.202306290.

[25] P. Martyniuk, P. Wang, A. Rogalski, Y. Gu, R. Jiang, F. Wang, W. Hu, Infrared avalanche photodiodes from bulk to 2D materials, Light Sci. Appl. 12 (1) (2023) 212, https://doi.org/10.1038/s41377-023-01259-3.

[26] R. Tian, X. Gan, C. Li, X. Chen, S. Hu, L. Gu, D. Van Thourhout, A. Castellanos-Gomez, Z. Sun, J. Zhao, Chip-integrated van Der Waals PN heterojunction photodetector with low dark current and high responsivity, Light Sci. Appl. 11 (1) (2022) 101, https://doi.org/10.1038/s41377-022-00784-x.

[27] H. Chaojian, L. Bo, L. Qingwei, Y. Lijun, W. Yang, Y. Zhan, D. Lixin, Plasmon-enhanced photovoltaic characteristics of black phosphorus-MoS_2 heterojunction, IEEE Open J. Nanotechnol. 2 (2021) 41–51, https://doi.org/10.1109/OJNANO.2021.3062495.

[28] A. Di Bartolomeo, Graphene schottky Diodes: an experimental review of the rectifying graphene/semiconductor heterojunction, Phys. Rep. 606 (2016) 1–58, https://doi.org/10.1016/j.physrep.2015.10.003.

[29] *Band alignment in black phosphorus/transition metal dichalcogenide heterolayers: impact of charge redistribution, electric field, strain, and layer engineering. J. Electron. Mater.*. doi:10.1007/s11664-022-10093-z (accessed 2024-01-28).

[30] C. Liu, S. Ding, Q. Tian, X. Hong, W. Su, L. Tang, L. Wang, M. Zhang, X. Liu, Y. Lv, J.C. Ho, L. Liao, X. Zou, Realizing the switching of optoelectronic memory and ultrafast detector in functionalized-black phosphorus/MoS_2 heterojunction, Laser & Photon. Rev. 17 (2) (2023) 2200486, https://doi.org/10.1002/lpor.202200486.

[31] *Engineering the Electron–Hole Bilayer Tunneling Field-Effect Transistor | IEEE Journals & Magazine | IEEE Xplore*. https://ieeexplore.ieee.org/abstract/document/6784495?casa_token=lyZfU4xWtUQAAAAA:rfv8DSQYpDt6BG5xloO4x-UOmAQF7wnEJ36jyINzfBabvHiQdtLBwycRJt_zRdKfjmODYOcdzA (accessed 2024-01-28).

[32] B. Koo, G.H. Shin, H. Park, H. Kim, S.-Y. Choi, Vertical-tunneling field-effect transistor based on MoTe2/MoS2 2D–2D heterojunction, J. Phys. D: Appl. Phys. 51 (47) (2018) 475101, https://doi.org/10.1088/1361-6463/aae2a7.

[33] E. Pollmann, A. Maas, D. Marnold, A. Hucht, R.-M. Neubieser, M. Stief, L. Madauß, M. Schleberger, Dynamic growth/etching model for the synthesis of two-dimensional transition metal dichalcogenides via chemical vapour deposition, 2D Mater. 9 (3) (2022) 035001, https://doi.org/10.1088/2053-1583/ac5ec5.

[34] E. Pollmann, L. Madauß, S. Schumacher, U. Kumar, F. Heuvel, C. Vom Ende, S. Yilmaz, S. Güngörmüs, M. Schleberger, Apparent differences between single layer molybdenum disulphide fabricated via chemical vapour deposition and exfoliation, Nanotechnology 31 (50) (2020) 505604, https://doi.org/10.1088/1361-6528/abb5d2.

[35] F. Urban, G. Lupina, A. Grillo, N. Martucciello, A. Di Bartolomeo, Contact resistance and mobility in back-gate graphene transistors, Nano Ex 1 (1) (2020) 010001, https://doi.org/10.1088/2632-959X/ab7055.

[36] A. Kumar, L. Viscardi, E. Faella, F. Giubileo, K. Intonti, A. Pelella, S. Sleziona, O. Kharsah, M. Schleberger, A. Di Bartolomeo, Temperature dependent black phosphorus transistor and memory, Nano Ex 4 (1) (2023) 014001, https://doi.org/10.1088/2632-959X/acbe11.

[37] A. Di Bartolomeo, A. Kumar, O. Durante, A. Sessa, E. Faella, L. Viscardi, K. Intonti, F. Giubileo, N. Martucciello, P. Romano, S. Sleziona, M. Schleberger, Temperature-dependent photoconductivity in two-dimensional MoS2 transistors, Mater. Today Nano 24 (2023) 100382, https://doi.org/10.1016/j.mtnano.2023.100382.

[38] S. Akcöltekin, M. El Kharrazi, B. Köhler, A. Lorke, M. Schleberger, Graphene on insulating crystalline substrates, Nanotechnology 20 (15) (2009) 155601, https://doi.org/10.1088/0957-4484/20/15/155601.

[39] J. Hopster, R. Kozubek, J. Krämer, V. Sokolovsky, M. Schleberger, Ultra-Thin MoS2 irradiated with highly charged ions, Nucl. Instrum. Methods Phys. Res., Sect. B 317 (2013) 165–169, https://doi.org/10.1016/j.nimb.2013.02.038.

[40] Simbulan, K.B.; Huang, T.-D.; Peng, G.-H.; Li, F.; Sanchez, O.J.G.; Lin, J.-D.; Qi, J.; Cheng, S.-J.; Lu, T.-H.; Lan, Y.-W. Twisted-light-revealed lightlike exciton dispersion in monolayer MoS2. arXiv January 5, 2020. doi:10.48550/arXiv.2001.01264.

[41] T.F.D. Fernandes, A.de C. Gadelha, A.P.M. Barboza, R.M. Paniago, L.C. Campos, P. S.S. Guimarães, P.-L.de Assis, B.R.A Neves, Robust nanofabrication of monolayer MoS2 islands with strong photoluminescence enhancement via local anodic oxidation, 2D Mater. 5 (2) (2018) 025018, https://doi.org/10.1088/2053-1583/aab38c.

[42] K.S. Kim, K.H. Kim, Y. Nam, J. Jeon, S. Yim, E. Singh, J.Y. Lee, S.J. Lee, Y.S. Jung, G.Y. Yeom, D.W. Kim, Atomic layer etching mechanism of MoS2 for nanodevices, ACS Appl. Mater. Interfaces 9 (13) (2017) 11967–11976, https://doi.org/10.1021/acsami.6b15886.

[43] L. Viscardi, K. Intonti, A. Kumar, E. Faella, A. Pelella, F. Giubileo, S. Sleziona, O. Kharsah, M. Schleberger, A. Di Bartolomeo, Black phosphorus nanosheets in field effect transistors with Ni and NiCr contacts, Physica Status Solidi (b) 260 (9) (2023) 2200537, https://doi.org/10.1002/pssb.202200537.

[44] H. Elhadidy, J. Sikula, J. Franc, Symmetrical current–voltage characteristic of a metal–semiconductor–metal structure of schottky contacts and parameter retrieval of a CdTe structure, Semicond. Sci. Technol. 27 (1) (2012) 015006, https://doi.org/10.1088/0268-1242/27/1/015006.

[45] A. Di Bartolomeo, A. Grillo, F. Urban, L. Iemmo, F. Giubileo, G. Luongo, G. Amato, L. Croin, L. Sun, S.-J. Liang, L.K. Ang, Asymmetric schottky contacts in bilayer MoS_2 field effect transistors, Adv. Funct. Mater. 28 (28) (2018) 1800657, https://doi.org/10.1002/adfm.201800657.

[46] A. Grillo, A. Di Bartolomeo, A current–voltage model for double schottky barrier devices, Adv. Electron. Mater. 7 (2) (2021) 2000979, https://doi.org/10.1002/aelm.202000979.

[47] O. Ochedowski, K. Marinov, N. Scheuschner, A. Poloczek, B.K. Bussmann, J. Maultzsch, M. Schleberger, Effect of contaminations and surface preparation on the work function of single layer MoS_2, Beilstein J. Nanotechnol. 5 (2014) 291–297, https://doi.org/10.3762/bjnano.5.32.

[48] J. Xiao, Y. Zhang, H. Chen, N. Xu, S. Deng, Enhanced performance of a monolayer MoS2/WSe2 heterojunction as a photoelectrochemical cathode, Nano-Micro Lett 10 (4) (2018) 60, https://doi.org/10.1007/s40820-018-0212-6.

[49] M.M. Furchi, A. Pospischil, F. Libisch, J. Burgdörfer, T. Mueller, Photovoltaic effect in an electrically tunable van der waals heterojunction, Nano Lett. 14 (8) (2014) 4785–4791, https://doi.org/10.1021/nl501962c.

[50] H. Yuan, Z. Li, Interfacial properties of black phosphorus/transition metal carbide van der waals heterostructures, Front. Phys. 13 (3) (2018) 138103, https://doi.org/10.1007/s11467-018-0759-1.

[51] L. Huang, N. Huo, Y. Li, H. Chen, J. Yang, Z. Wei, J. Li, S.-S. Li, Electric-field tunable band offsets in black phosphorus and MoS2 van der waals p-n heterostructure, J. Phys. Chem. Lett. 6 (13) (2015) 2483–2488, https://doi.org/10.1021/acs.jpclett.5b00976.

[52] P. Chen, J. Xiang, H. Yu, J. zhang, G. Xie, S. Wu, X. Lu, G. Wang, J. Zhao, F. Wen, Z. Liu, R. Yang, D. Shi, G. Zhang, Gate tunable MoS2–black phosphorus heterojunction devices, 2D Mater. 2 (3) (2015) 034009, https://doi.org/10.1088/2053-1583/2/3/034009.

[53] H.B. Michaelson, The work function of the elements and its periodicity, J. Appl. Phys. 48 (11) (1977) 4729–4733, https://doi.org/10.1063/1.323539.

[54] A. Grillo, A. Pelella, E. Faella, F. Giubileo, S. Sleziona, O. Kharsah, M. Schleberger, A. Di Bartolomeo, Memory effects in black phosphorus field effect transistors, 2D Mater. 9 (1) (2022) 015028, https://doi.org/10.1088/2053-1583/ac3f45.

[55] le F. Telesio, G. Gal, M. Serrano-Ruiz, F. Prescimone, S. Toffanin, M. Peruzzini, S. Heun, Ohmic contact engineering in few–layer black phosphorus: approaching the quantum limit, Nanotechnology 31 (33) (2020) 334002, https://doi.org/10.1088/1361-6528/ab8cf4.

[56] B. Jiang, X. Zou, J. Su, J. Liang, J. Wang, H. Liu, L. Feng, C. Jiang, F. Wang, J. He, L. Liao, Impact of thickness on contact issues for pinning effect in black phosphorus field-effect transistors, Adv. Funct. Mater. 28 (26) (2018) 1801398, https://doi.org/10.1002/adfm.201801398.

[57] J.-Y. Wu, Y.T. Chun, S. Li, T. Zhang, D. Chu, Electrical rectifying and photosensing property of schottky diode based on MoS2, ACS Appl. Mater. Interfaces 10 (29) (2018) 24613–24619, https://doi.org/10.1021/acsami.8b06078.

[58] Y. Pan, J. Gu, H. Tang, X. Zhang, J. Li, B. Shi, J. Yang, H. Zhang, J. Yan, S. Liu, H. Hu, M. Wu, J. Lu, Reexamination of the schottky barrier heights in monolayer MoS2 field-effect transistors, ACS Appl. Nano Mater. 2 (8) (2019) 4717–4726, https://doi.org/10.1021/acsanm.9b00200.

[59] A. Kumar, L. Viscardi, E. Faella, F. Giubileo, K. Intonti, A. Pelella, S. Sleziona, O. Kharsah, M. Schleberger, A. Di Bartolomeo, Black phosphorus unipolar transistor, memory, and photodetector, J. Mater. Sci. 58 (6) (2023) 2689–2699, https://doi.org/10.1007/s10853-023-08169-0.

[60] K. Intonti, E. Faella, A. Kumar, L. Viscardi, F. Giubileo, N. Martucciello, H.T. Lam, K. Anastasiou, M. Craciun, S. Russo, A. Di Bartolomeo, Temperature-dependent conduction and photoresponse in few-layer ReS_2, ACS Appl. Mater. Interfaces 15 (43) (2023) 50302–50311, https://doi.org/10.1021/acsami.3c12973.